

# *Swift* follow-up of the Gravitational Wave source GW150914

P.A. Evans<sup>1\*</sup>, J.A. Kennea<sup>2</sup>, S.D. Barthelmy<sup>3</sup>, D. N. Burrows<sup>2</sup>, S. Campana<sup>4</sup>,  
S.B. Cenko<sup>3,5</sup>, N. Gehrels<sup>3</sup>, P. Giommi<sup>6</sup>, F. E. Marshall<sup>3</sup>, J. A. Nousek<sup>2</sup>,  
P. T. O’Brien<sup>1</sup>, J. P. Osborne<sup>1</sup>, D.M. Palmer<sup>7</sup>, M. Perri<sup>6,8</sup>, J. L. Racusin<sup>3</sup>,  
M.H. Siegel<sup>2</sup>, G. Tagliaferri<sup>4</sup>

<sup>1</sup> Department of Physics and Astronomy, University of Leicester, Leicester, LE1 7RH, UK

<sup>2</sup> Department of Astronomy and Astrophysics, Pennsylvania State University, 525 Davey Lab, University Park, PA 16802, USA

<sup>3</sup> NASA Goddard Space Flight Center, Mail Code 661, Greenbelt, MD 20771, USA

<sup>4</sup> INAF, Osservatorio Astronomico di Brera, via E. Bianchi 46, 23807 Merate, Italy

<sup>5</sup> Joint Space-Science Institute, University of Maryland, College Park, MD 20742, USA

<sup>6</sup> Agenzia Spaziale Italiana (ASI) Science Data Center, I-00133 Roma, Italy;

<sup>7</sup> Los Alamos National Laboratory, B244, Los Alamos, NM, 87545, USA

<sup>8</sup> INAF-Osservatorio Astronomico di Roma, via Frascati 33, I-00040 Monteporzio Catone, Italy

Accepted – Received –

## ABSTRACT

The Advanced LIGO observatory recently reported the first direct detection of gravitational waves. We report on observations taken with the *Swift* satellite two days after the GW trigger. No new X-ray, optical, UV or hard X-ray sources were detected in our observations, which were focussed on nearby galaxies in the gravitational wave error region and we discuss the implications of this.

## Key words:

## 1 INTRODUCTION

The Advanced LIGO (ALIGO) observatory (LIGO Scientific Collaboration et al. 2015) recently reported the first ever direct detection of gravitational waves (GW; Abbott et al. 2016), ALIGO event GW150914. One of the most likely sources of gravitational waves detectable by ALIGO comes from the coalescence of a compact binary, i.e. one containing neutron stars (NS) or stellar-mass black holes (BH). Such events may well be accompanied by transient electromagnetic (EM) radiation such as a short gamma ray burst (if the binary is viewed close to face-on) or a kilonova (see, e.g. Metzger & Berger 2012; Cowperthwaite & Berger 2015). In a previous work (Evans et al. 2016; hereafter ‘Paper I’) we discussed how the *Swift* satellite (Gehrels et al. 2004) could respond to such triggers to search for emission from a short GRB afterglow with the X-ray telescope (XRT; Burrows et al. 2005). *Swift* was able to rapidly respond and provide the first follow-up reports.

The ‘Coherent WaveBurst’ (cWB) pipeline for ALIGO triggered on 2015 September 14 at 09:50:45 UT, reporting a

signal with a false alarm rate of  $1.178 \times 10^{-8}$  Hz, i.e. a spurious signal of this significance is expected once every 2.7 years (this was later revised to less than one every four hundred years; LIGO Scientific Collaboration 2015b and then one per 203,000 years, Abbott et al. 2016). This event was announced to the EM follow-up partners on 2015 September 16 at 06:39 UT (Singer 2015). The 90% confidence error region in the initially-released skymap ‘LIB-skymap’ covered 750 square degrees (this was later reduced to 600 square degrees in the ‘LALInterence’ skymap; LIGO Scientific Collaboration 2015a). In this letter we report on follow-up observations with the XRT and UV/Optical telescope (UVOT; Roming et al. 2005), and we also searched the Burst Alert Telescope (BAT; Barthelmy et al. 2005) data for any sign of hard X-ray emission at the time of the trigger. A summary of all of the EM follow-up of GW150914 was given by the LIGO-EM follow up team (2016, this arXiv listing).

Throughout this paper, errors are quoted at the 90% confidence level unless otherwise stated, and all fluxes are the observed flux (as opposed to unabsorbed).

\* pae9@leicester.ac.uk

## 2 *Swift* OBSERVATIONS

While Paper I advocated a large-scale rapid tiling with *Swift* in response to a GW trigger, such an operating mode had not been commissioned when ALIGO triggered on GW150914<sup>1</sup>, therefore we were obliged to observe a smaller number of fields. Following Paper I we convolved the ALIGO sky localisation map (we used the ‘LIB\_skymap’ which was the best map available at time of our observations; Abbott et al. 2016) with the GWGC galaxy catalogue (White, Daw & Dhillon 2011). We added a 100 kpc halo to each galaxy in the GWGC more than 5 Mpc away<sup>2</sup>, to reflect possible impact of natal NS kicks. However, unlike our previous work (where pixels in this map had values of 1 or 0) we weighted this map by galaxy luminosity. Each GWGC galaxy was assigned a probability  $P = L/L_{\text{tot}}$ , where  $L$  is the B-band luminosity of the galaxy reported in the GWGC and  $L_{\text{tot}}$  is the total luminosity of all galaxies in the catalogue. This probability was then evenly distributed between all HEALPIX<sup>3</sup> pixels corresponding to the galaxy and its halo, i.e. we assume that the probability of a binary neutron star merger (which gives rise to the GRB and GW emission) is spatially uniform throughout the host galaxy and its halo.

The LIB\_skymap from the ALIGO team and the version convolved with GWGC are shown in Fig. 1. Unfortunately a large portion of the error region was within *Swift*’s Sun observing constraint where we cannot observe ( $< 47^\circ$  from the Sun). Gehrels et al. (2015) noted that, since most of the galaxy luminosity comes from a small fraction of galaxies, one can opt to only observe the brightest galaxies within the ALIGO error region; Kasliwal et al. (2015) reported a list of such galaxies. Unfortunately, three of their top ten were within the Sun constraint region.

Rather than select where to point based on individual galaxies, we divided the observable sky into XRT fields of view (since one field may contain multiple galaxies) and ranked them in decreasing order of probability derived from our GWGC-convolved skymap, and then observed the top five fields from this list, which contained eight GWGC galaxies. Noting that the GW error region also intersected the Large Magellanic Cloud (LMC), we also performed a 37-point tiled observation focussed on the LMC (Fig. 2). This tiling formed part of the process of commissioning the ability to observe as Paper I advocated, and as it was the first such test, we were limited to short exposures. A full list of the *Swift* observations is given in Table 1.

## 3 DATA ANALYSIS

The XRT data analysis was largely automated, using custom software produced by (and running at) the UK Swift Science Data Centre at the University of Leicester. This software

<sup>1</sup> The trigger actually occurred at the end of an engineering run, before the official start of the O1 observing run.

<sup>2</sup> For galaxies closer than this 5 Mpc, the angular projection of a 100 kpc halo covers an unreasonably large fraction of the sky, but the fraction of binary NS mergers which occur within this distance is negligible

<sup>3</sup> Hierarchical Equal Area isoLatitude Pixelization (Górski et al. 2005), the file format in which ALIGO error regions are disseminated.

**Table 1.** *Swift* observations of the error region of GW150914

Pointing direction (J2000)	Start time <sup>a</sup> (UTC)	Exposure (s)
09 <sup>h</sup> 13 <sup>m</sup> 29.65 <sup>s</sup> , −60°43′37.4″	Sep 16 at 15:19:27	777
08 <sup>h</sup> 16 <sup>m</sup> 30.77 <sup>s</sup> , −67°38′06.7″	Sep 16 at 16:54:41	987
07 <sup>h</sup> 28 <sup>m</sup> 42.38 <sup>s</sup> , −66°59′43.1″	Sep 16 at 18:28:32	970
08 <sup>h</sup> 03 <sup>m</sup> 23.72 <sup>s</sup> , −67°37′17.2″	Sep 16 at 20:05:37	970
08 <sup>h</sup> 57 <sup>m</sup> 17.34 <sup>s</sup> , −65°26′34.1″	Sep 16 at 21:42:15	985
LMC Observations		
06 <sup>h</sup> 55 <sup>m</sup> 30.59 <sup>s</sup> , −68°18′44.3″	Sep 17 at 18:26:54	20
06 <sup>h</sup> 59 <sup>m</sup> 13.43 <sup>s</sup> , −68°18′29.7″	Sep 17 at 18:28:03	42
06 <sup>h</sup> 57 <sup>m</sup> 21.25 <sup>s</sup> , −68°36′12.8″	Sep 17 at 18:29:12	20
06 <sup>h</sup> 53 <sup>m</sup> 42.84 <sup>s</sup> , −68°36′04.4″	Sep 17 at 18:30:21	22
06 <sup>h</sup> 51 <sup>m</sup> 53.97 <sup>s</sup> , −68°18′16.7″	Sep 17 at 18:31:29	32
06 <sup>h</sup> 53 <sup>m</sup> 45.48 <sup>s</sup> , −68°00′43.4″	Sep 17 at 18:32:38	22
06 <sup>h</sup> 57 <sup>m</sup> 25.10 <sup>s</sup> , −68°01′02.6″	Sep 17 at 18:33:46	25
07 <sup>h</sup> 01 <sup>m</sup> 1.84 <sup>s</sup> , −68°01′05.6″	Sep 17 at 18:34:54	35
07 <sup>h</sup> 02 <sup>m</sup> 52.89 <sup>s</sup> , −68°18′56.6″	Sep 17 at 18:36:02	72
07 <sup>h</sup> 01 <sup>m</sup> 05.50 <sup>s</sup> , −68°36′16.1″	Sep 17 at 18:37:09	82
06 <sup>h</sup> 59 <sup>m</sup> 11.14 <sup>s</sup> , −68°53′42.6″	Sep 17 at 18:38:17	37
06 <sup>h</sup> 55 <sup>m</sup> 32.45 <sup>s</sup> , −68°53′32.4″	Sep 17 at 18:39:25	25
06 <sup>h</sup> 51 <sup>m</sup> 54.75 <sup>s</sup> , −68°53′32.0″	Sep 17 at 18:40:33	65
06 <sup>h</sup> 50 <sup>m</sup> 5.28 <sup>s</sup> , −68°35′51.8″	Sep 17 at 18:41:40	52
06 <sup>h</sup> 48 <sup>m</sup> 15.62 <sup>s</sup> , −68°18′20.6″	Sep 17 at 18:42:47	65
06 <sup>h</sup> 50 <sup>m</sup> 6.94 <sup>s</sup> , −68°00′54.0″	Sep 17 at 18:43:53	60
06 <sup>h</sup> 51 <sup>m</sup> 56.98 <sup>s</sup> , −67°43′22.9″	Sep 17 at 18:44:59	67
06 <sup>h</sup> 55 <sup>m</sup> 34.08 <sup>s</sup> , −67°43′36.1″	Sep 17 at 18:46:04	72
06 <sup>h</sup> 59 <sup>m</sup> 13.52 <sup>s</sup> , −67°43′33.4″	Sep 17 at 18:47:10	55
07 <sup>h</sup> 02 <sup>m</sup> 51.97 <sup>s</sup> , −67°43′41.4″	Sep 17 at 18:48:15	62
07 <sup>h</sup> 04 <sup>m</sup> 42.41 <sup>s</sup> , −68°01′15.1″	Sep 17 at 18:49:21	75
07 <sup>h</sup> 06 <sup>m</sup> 30.83 <sup>s</sup> , −68°18′50.4″	Sep 17 at 18:50:27	70
07 <sup>h</sup> 04 <sup>m</sup> 41.09 <sup>s</sup> , −68°36′37.2″	Sep 17 at 18:51:32	60
07 <sup>h</sup> 02 <sup>m</sup> 50.35 <sup>s</sup> , −68°53′43.9″	Sep 17 at 18:52:38	60
07 <sup>h</sup> 01 <sup>m</sup> 1.00 <sup>s</sup> , −69°11′19.8″	Sep 17 at 18:53:43	62
06 <sup>h</sup> 57 <sup>m</sup> 21.83 <sup>s</sup> , −69°11′05.0″	Sep 17 at 18:54:49	67
06 <sup>h</sup> 53 <sup>m</sup> 43.60 <sup>s</sup> , −69°11′06.9″	Sep 17 at 18:55:55	42
06 <sup>h</sup> 50 <sup>m</sup> 4.65 <sup>s</sup> , −69°11′01.6″	Sep 17 at 20:02:45	20
06 <sup>h</sup> 48 <sup>m</sup> 14.61 <sup>s</sup> , −68°53′22.8″	Sep 17 at 20:03:54	32
06 <sup>h</sup> 46 <sup>m</sup> 25.66 <sup>s</sup> , −68°35′44.9″	Sep 17 at 20:05:02	20
06 <sup>h</sup> 44 <sup>m</sup> 35.32 <sup>s</sup> , −68°18′21.1″	Sep 17 at 20:06:11	25
06 <sup>h</sup> 46 <sup>m</sup> 27.88 <sup>s</sup> , −68°00′48.6″	Sep 17 at 20:07:19	35
06 <sup>h</sup> 48 <sup>m</sup> 17.47 <sup>s</sup> , −67°43′23.8″	Sep 17 at 20:08:27	60
06 <sup>h</sup> 50 <sup>m</sup> 7.30 <sup>s</sup> , −67°25′50.9″	Sep 17 at 20:09:34	70
06 <sup>h</sup> 53 <sup>m</sup> 44.83 <sup>s</sup> , −67°26′05.6″	Sep 17 at 20:10:41	77
06 <sup>h</sup> 57 <sup>m</sup> 24.51 <sup>s</sup> , −67°26′04.1″	Sep 17 at 20:11:48	67
07 <sup>h</sup> 01 <sup>m</sup> 2.66 <sup>s</sup> , −67°26′08.1″	Sep 17 at 20:12:54	57

<sup>a</sup> All observations were in 2015.

makes extensive use of the *Swift* software (v4.3<sup>4</sup>) with the latest CALDB files<sup>5</sup>.

Our baseline source detection system was that developed by Evans et al. (2014) for the 1 Swift XRT Point Source (1SXPS) catalogue. This is an iterative system, that uses a sliding-cell detection method with a background map which is recreated on each pass to account for sources already discovered. The majority of datasets in the 1SXPS catalogue corresponded to a single XRT field of view, and even where multiple fields of view overlapped, images were limited to

<sup>4</sup> Part of HEASOFT 6.15.1

<sup>5</sup> Released on 2015 July 21.

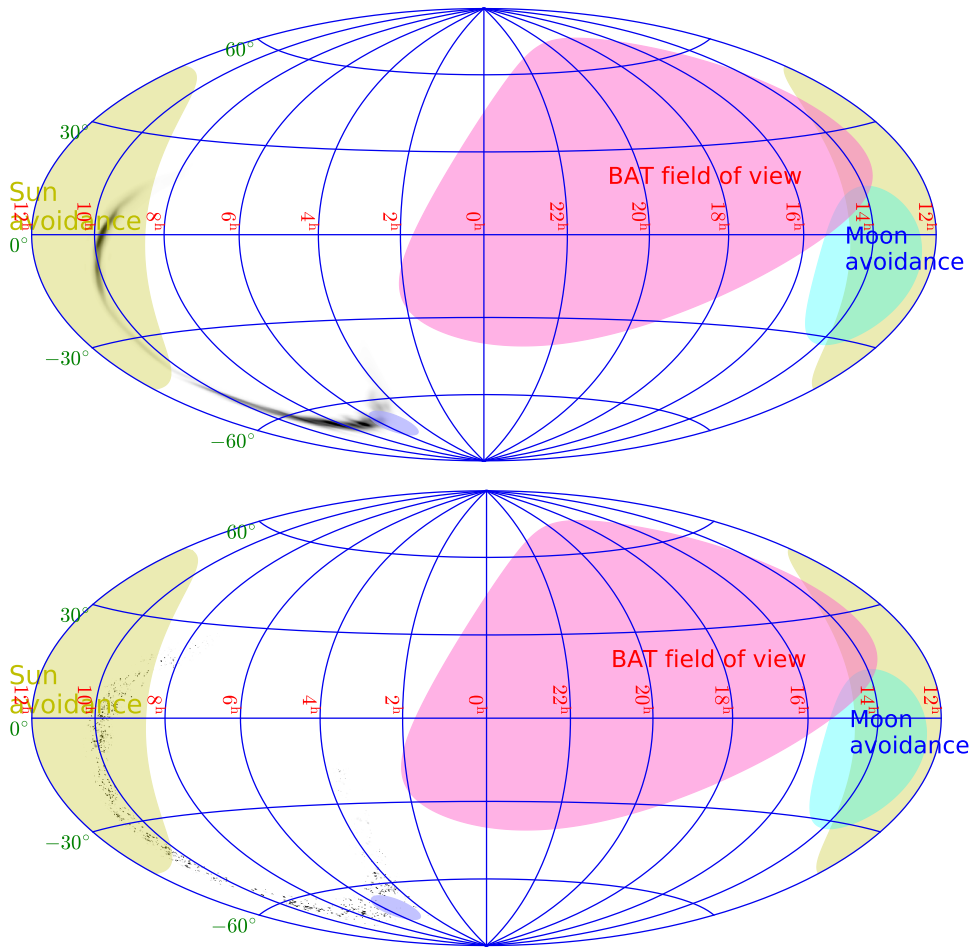


**Figure 1.** The ‘LIB\_skymap’ GW localisation map produced by the LVC team on 2015 September 15 (top), convolved with our luminosity-weighted GWGC map (bottom). Coordinates are equatorial, J2000. The yellow and cyan circles show the regions of the sky which *Swift* could not observe due to the presence of the sun and moon respectively, calculated at the time of the first *Swift* observations. The small, pale lilac ellipse marks the LMC. The large purple region approximates the BAT field of view at the time of the GW trigger.

1000×1000 pixels ( $39.3' \times 39.3'$ ) in size. For GW150914 we observed a large contiguous region (part of the LMC; Fig. 2) – this region is so large that the background mapping developed for 1SXPS is not properly calibrated, and the coordinates in the tangent-plane projection become inaccurate. We therefore broke the data into ‘analysis blocks’. Each block was no more than  $0.55^\circ$  in radius (equivalent to a 7-point tile), and every XRT field of view had to be in at least one block. Any redundant blocks (i.e. where every XRT field in the block was also in another block) were removed. Since this meant that some areas of sky were in multiple blocks, we checked for duplicate detections of the same source (based on spatial coincidence) from multiple blocks and merged any that occurred.

In 1SXPS the minimum exposure time permitted was 100 s, however Table 1 shows that many of the observations (those of the LMC) were shorter than this. This is not likely to be a problem regarding spurious source detections; Evans et al. (2014) found that at short exposure times there are very few spurious sources due to the lack of background events. However, this lack of background may mean that we can reduce the signal-to-noise ratio (S/N) threshold

for sources to be accepted in short exposure. We simulated 50-s exposure images (both single fields, and 7-point tiles, to represent the extreme sizes of the analysis blocks) in a manner analogous to Evans et al. (2014) and found that for an S/N threshold of 1.3, the rate of spurious detections was  $< 3/1000$ , equivalent to the ‘Good’ flag in 1SXPS.

As discussed in Paper I, the discovery of an X-ray source alone does not identify it as the counterpart to the GW trigger. We therefore gave each detected source a ‘rank’ indicating how likely it is to be related to the GW event, from 1 (very likely) to 4 (very unlikely). This involved comparing our source detections with the *ROSAT* All Sky Survey (RASS; Voges et al. 1999). To do this we assumed a typical AGN spectrum, a power-law with  $N_H = 3 \times 10^{20} \text{ cm}^{-2}$  and a photon index of  $\Gamma = 1.7$ . These ranks were defined as follows:

*Rank 1: Good GW counterpart candidate.* Sources which lie within 200 kpc of a GWGC galaxy, and are either uncatalogued and brighter than the  $3\text{-}\sigma$  catalogue limit, or catalogued but brighter than their catalogued flux. In both cases, ‘brighter than’ means that the measured and historical values (or upper limits) disagree at the  $5\text{-}\sigma$  level. For uncata-

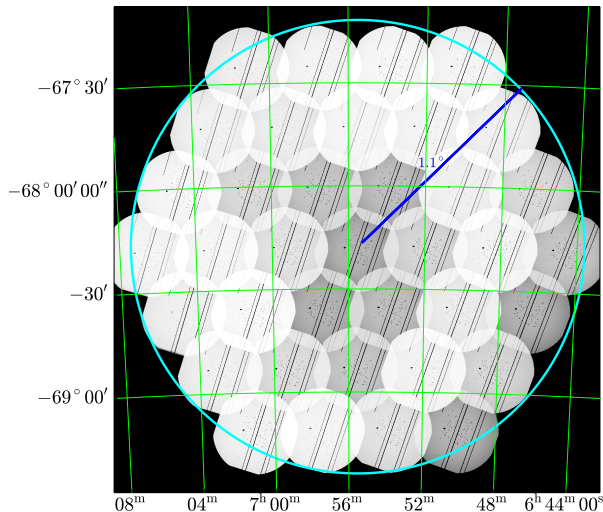


**Figure 2.** The exposure map of the 37-point tiled observations of the LMC performed with *Swift*, demonstrating the structure of the pattern. The black lines are the vetoed columns on the CCD. The cyan circle has radius of  $1.1^\circ$  and is shown for reference.

logged sources, the comparison is to the RASS, or to 1SXPS or the XMM catalogues, if an upper limit from those catalogues is available and deeper than the RASS limit.

*Rank 2: Possible counterpart.* The criteria for this are similar to those above, except that ‘brighter’ is determined at the  $3\text{-}\sigma$  level, and there is no requirement for the source to be near a known galaxy.

*Rank 3: Undistinguished source.* Sources which are uncatalogued, but are fainter than existing catalogue limits, or consistent with those limits at the  $3\text{-}\sigma$  level. i.e. sources which cannot be distinguished from field sources.

*Rank 4: Not a counterpart.* Sources which are catalogued, and which have fluxes consistent with (at the  $3\text{-}\sigma$  level) or fainter than their catalogued values.

The relatively conservative flux requirements of rank 1 arise because of biases which cause us to overestimate the ratio between the observed flux and historical flux or limit. The Eddington bias (Eddington 1940) results in the fluxes of sources close to the detection limit being overestimated; this was discussed and quantified for *Swift* by Evans et al. (2014) (section 6.2.1 and figs. 9–10). Also, *ROSAT* had a much softer response than *Swift* (0.1–2.4 keV compared to 0.3–10 keV); for sources with harder spectra than in our assumed model (especially those more heavily absorbed) this means that *ROSAT* was less sensitive, i.e. our calculated XRT/*ROSAT* ratio will be too low.

As well as the checks performed to automatically rank each XRT source, the 2MASS catalogue (Skrutskie et al. 2006) and SIMBAD database (Wenger et al. 2000) were automatically searched, and any sources within the  $3\text{-}\sigma$  XRT error region were identified. This information was not used to determine the source rank, but to inform human decisions as to the nature of the source. It is important to note that this spatial correlation does not necessarily mean that the XRT source and the 2MASS/SIMBAD object are the same thing: Evans et al. (2014) showed that  $\sim 11\%$  of XRT

sources with SIMBAD matches, and  $\sim 64\%$  of those with 2MASS matches are not related but chance alignments.

An automated pipeline was built to search for candidate counterparts in the UVOT observations using standard HEASOFT analysis tools. In the pipeline the tool UVOTDETECT was used to search for sources in the sky image files. For each observation searches were made using the longest exposure and the sum of all images if the summed exposure was significantly longer than the longest exposure. Candidate sources whose images were not star-like or were too close to other sources were rejected. Sources without counterparts in the Digital Sky Survey (DSS) or Hubble Guide Star Catalog (GSC) were considered possible candidates. The UVOT image near each of these possible candidates was then visually compared with the corresponding region in the DSS. This visual comparison was used to reject candidates due to readout streaks or ghost images of bright sources.

The UVOT images near Rank 1 or Rank 2 XRT sources were also examined and compared with the DSS. UVOT source magnitudes or upper limits were determined using the tool uvotsource.

## 4 RESULTS

Three X-ray objects were found in the initial observations (the five most probable XRT fields) and announced by Evans et al. (2015). These were all known X-ray emitters showing no sign of outburst and assigned a rank of 4, see Table 2 for details. Source 2 was automatically flagged as being potentially spurious due to optical loading as it is spatially coincident with HD 79905 which SIMBAD reports as a B9.5 star (Houk & Cowley 1975) with a V magnitude of 7.436 (Kiraga 2012), above the threshold where optical loading is likely to affect the X-ray measurements<sup>6</sup>. The measured count-rate ( $0.045 \pm 0.011$  ct/sec) is however slightly lower than that in the RASS ( $0.10 \pm 0.01$  ct/sec when converted to an XRT-equivalent rate using the AGN spectrum introduced above), suggesting that the optical loading has not resulted in a spurious X-ray detection.

The  $3\text{-}\sigma$  upper limit on any other X-ray point source in the initial five fields is  $1.5 \times 10^{-2}$  ct/sec, which corresponds to a flux of  $6.5 \times 10^{-13}$  erg  $\text{cm}^{-2}$   $\text{s}^{-1}$ , assuming the AGN spectrum defined above. For the LMC observations the typical upper limit was 0.16 ct/sec, or  $6.9 \times 10^{-12}$  erg  $\text{cm}^{-2}$   $\text{s}^{-1}$ .

UVOT observations were all carried out in the *u* filter, 2 of the sources were detected and one lay outside the field of view. Details are in Table 2. No transient sources were detected by UVOT down to an AB magnitude of 19.9.

The ALIGO sky localisation was outside of BATs nominal Field-Of-View, but BAT often detects gamma ray bursts from outside of the field of view, through gamma-rays that leak through the sidewall shielding. A search for any corresponding rate increases from a correlated GRB within  $\pm 100$  seconds of the gravitational wave signal found no peaks above the  $3\text{-}\sigma$  value of 200 ct/sec above background in the nominally 50–300 keV energy range at a 1-second timescale.

<sup>6</sup> <http://www.swift.ac.uk/analysis/xrt/optical.tool.php>

**Table 2.** Sources detected by *Swift* follow-up of GW150914

RA (J2000)	Dec (J2000)	Error 90% conf.	Flux 0.3–10 keV, erg cm <sup>-2</sup> s <sup>-1</sup>	Magnitude AB mag	Catalogued name
09h 14m 06.54s	-60° 32′ 07.7″	4.8″	$(1.9 \pm 0.5) \times 10^{-12}$	N/A	XMMSL1 J091406.5-603212
09h 13m 30.24s	-60° 47′ 18.1″	6.1″	$(5.3 \pm 2.0) \times 10^{-13}$	15.44±0.02 <sup>a</sup>	ESO 126-2 = 1RXS J091330.1-604707
08h 17m 60.62s	-67° 44′ 03.9″	4.7″	$(8.9 \pm 2.4) \times 10^{-13}$	17.53±0.05	1RXS J081731.6-674414

<sup>a</sup> Magnitude of the core. The galaxy as a whole (removing foreground stars) has a *u* magnitude of 14.15±0.02.

## 5 DISCUSSION AND CONCLUSIONS

The XRT observations covered 4.7 square degrees, and contained 2% of the probability from the final ‘LALInterence’ ALIGO error region (8% if this is convolved with the GWGC). However, Abbott et al. (2016) reported that the most likely source of the GW event is a binary black-hole trigger at 500 Mpc. Since the GWGC only extends to 100 Mpc and the coalescence of two stellar mass black holes is not expected to produce EM radiation, our lack of detection is not surprising.

*Fermi*-GBM reported a possible low significance gamma-ray event coincident with the ALIGO trigger (Blackburn et al. 2015), Connaughton et al (2016, this arXiv listing), although this was not detected by INTEGRAL (Ferrigno et al. 2015). No corresponding signal was seen by the *Swift*-BAT, however since none of the ALIGO error region was in the BAT field of view at the time of the trigger, this is not surprising.

Although the *Swift* observations did not yield the detection of an EM counterpart to the GW trigger, we have demonstrated that we are able to respond very rapidly to GW triggers with *Swift*: the 3 X-ray sources we detected were reported to the GW-EM community within 15 hours of the trigger being announced. In the event of a nearby binary neutron-star merger triggering ALIGO, such rapid response, analysis and dissemination will be vital. It is also evident that the decisions made regarding where to observe with *Swift* are best informed if details such as estimated distances and masses are available rapidly from the GW teams, as noted by the GW-EM summary paper (this arXiv mailing), and it is expected that the latencies in deriving these parameters will be reduced in the future. We have also commissioned new observing modes with *Swift* which will allow us to perform much more extensive follow-up observations of future GW triggers.

## ACKNOWLEDGEMENTS

This work made use of data supplied by the UK Swift Science Data Centre at the University of Leicester, and used the ALICE High Performance Computing Facility at the University of Leicester. This research has made use of the XRT Data Analysis Software (XRTDAS) developed under the responsibility of the ASI Science Data Center (ASDC), Italy. PAE and JPO acknowledge UK Space Agency support. SC and GT acknowledge Italian Space Agency support. This publication makes use of data products from the Two Micron All Sky Survey, which is a joint project of the University of Massachusetts and the Infrared Process-

ing and Analysis Center/California Institute of Technology, funded by the National Aeronautics and Space Administration and the National Science Foundation, and the SIMBAD database, operated at CDS, Strasbourg, France.

## REFERENCES

- Abbott B. P. et al., 2016, *Phys. Rev. Lett.*, 116, 061102  
 Barthelmy S. D. et al., 2005, *Space Sci. Rev.*, 120, 143  
 Blackburn L. et al., 2015, GRB Coordinates Network, 18339  
 Burrows D. N. et al., 2005, *Space Sci. Rev.*, 120, 165  
 Cowperthwaite P. S., Berger E., 2015, *ApJ*, 814, 25  
 Eddington, Sir A. S., 1940, *MNRAS*, 100, 354  
 Evans P. A. et al., 2015, GRB Coordinates Network, 18331  
 Evans P. A. et al., 2014, *ApJS*, 210, 8  
 Evans P. A. et al., 2016, *MNRAS*, 455, 1522  
 Ferrigno C., Savchenko V., Mereghetti S., Kuulkers E., Bazzano A., Bozzo E., Courvosier T. J.-L., 2015, GRB Coordinates Network, 18354  
 Gehrels N., Cannizzo J. K., Kanner J., Kasliwal M. M., Nissanke S., Singer L. P., 2015, *ArXiv e-prints*  
 Gehrels N. et al., 2004, *ApJ*, 611, 1005  
 Górski K. M., Hivon E., Banday A. J., Wandelt B. D., Hansen F. K., Reinecke M., Bartelmann M., 2005, *ApJ*, 622, 759  
 Houk N., Cowley A. P., 1975, University of Michigan Catalogue of two-dimensional spectral types for the HD stars. Volume I. Declinations -90\_ to -53\_f0.  
 Kasliwal M. M., Cannizzo J. K., Gehrels N., Evans P., 2015, GRB Coordinates Network, 18340  
 Kiraga M., 2012, *Acta Astron.*, 62, 67  
 LIGO Scientific Collaboration, 2015a, GRB Coordinates Network, 18858  
 LIGO Scientific Collaboration, 2015b, GRB Coordinates Network, 18851  
 LIGO Scientific Collaboration et al., 2015, *Classical and Quantum Gravity*, 32, 074001  
 Metzger B. D., Berger E., 2012, *Astrophys. J.*, 746, 48  
 Roming P. W. A. et al., 2005, *Space Sci. Rev.*, 120, 95  
 Singer L., 2015, GRB Coordinates Network, 18330  
 Skrutskie M. F. et al., 2006, *AJ*, 131, 1163  
 Voges W. et al., 1999, *A&A*, 349, 389  
 Wenger M. et al., 2000, *A&AS*, 143, 9  
 White D. J., Daw E. J., Dhillon V. S., 2011, *Class. Quantum Gravity*, 28, 085016